Fuel 88 (2009) 1547–1553

Contents lists available at ScienceDirect

Fuel

journal homepage: www.elsevier.com/locate/fuel

# Ni catalysts with Mo promoter for methane steam reforming

S.S. Maluf, E.M. Assaf *

*Instituto de Química de São Carlos, Universidade de São Paulo, Av. Trabalhador São Carlense, 400 São Carlos, SP 13560-970, Brazil*

ARTICLE INFO

*Article history:*
Received 3 October 2008
Received in revised form 12 March 2009
Accepted 19 March 2009
Available online 9 April 2009

*Keywords:*
Methane steam reforming
Ni catalysts
Mo promoter

ABSTRACT

$NiO/Al_2O_3$ catalyst precursors were prepared by simultaneous precipitation, in a Ni:Al molar ratio of 3:1, promoted with Mo oxide (0.05, 0.5, 1.0 and 2.0 wt%). The solids were characterized by adsorption of $N_2$, XRD, TPR, Raman spectroscopy and XPS, then activated by $H_2$ reduction and tested for the catalytic activity in methane steam reforming.

The characterization results showed the presence of NiO and $Ni_2AlO_4$ in the bulk and $Ni_2AlO_4$ and/or $Ni_2O_3$ and $MoO_4^{-2}$ at the surface of the samples.

In the catalytic tests, high stability was observed with a reaction feed of 4:1 steam/methane. However, at a steam/methane ratio of 2:1, only the catalyst with 0.05% Mo remained stable throughout the 500 min of the test.

The addition of Mo to Ni catalysts may have a synergistic effect, probably as a result of electron transfer from the molybdenum to the nickel, increasing the electron density of the catalytic site and hence the catalytic activity.



## 1. Introduction

Hydrogen is an attractive energy carrier because it can be combusted, like gasoline and natural gas, or converted to electricity in a fuel cell, without any carbon emissions at the point of use [1–3]. The demand for hydrogen as a major feedstock in the chemical, petroleum refining and petrochemical industries is also growing [2,4].

Currently, 80–85% of all hydrogen supplied in the world is produced by methane steam reforming (MSR) [1], because of the abundance of natural gas (main source of methane) and its economic advantage over other processes.

The reaction of methane steam reforming [2,4] is:

$$CH_4 + 2H_2O \leftrightarrows CO_2 + 4H_2 \quad \Delta H^0_{298\,K} = 165\ \mathrm{kJ\ mol^{-1}}$$

This process is highly endothermic. To achieve a high conversion of methane and to avoid carbon deposition by methane cracking (reaction (1)) or by disproportionation of CO reaction (reaction (2)), steam is introduced in excess, leading to high energy consumption:

$$CH_4 \leftrightarrows C + 2H_2 \quad \Delta H^0_{298\,K} = 75\ \mathrm{kJ\ mol^{-1}} \qquad (1)$$

$$2CO \leftrightarrows CO_2 + C \quad \Delta H^0_{298\,K} = 86.2\ \mathrm{kJ\ mol^{-1}} \qquad (2)$$

Nickel-rich $Ni–Al_2O_3$ catalysts have proved to be highly active for MSR; this is attributed to strong and uniform interactions in the $Ni–Al_2O_3$ catalyst. However, the stability of the catalysts declines with increasing temperature and coke formation [5–7].

Some investigations have shown that the presence of a third component could improve the stability of catalysts at high temperatures, with little or no coking deactivation and with a high activity that simultaneously offers an increase in the yield of hydrogen [8,9].

Specifically, it was reported that a Ni catalyst, made by modifying commercial $Ni/Al_2O_3$ catalysts with a small amount of Mo [10], showed stable catalytic performance in the cracking, hydrogenolysis [11] and steam reforming of *n*-butane [12], because the addition of Mo not only decreases the rate of coking but also extends the beginning of coking.

The bases of the above information, in this study, $Mo–Ni/Al_2O_3$ catalysts were prepared, characterized (ICP, BET, XRD, TPR, Raman Spectroscopy and XPS) and tested in methane steam reforming, to investigate the stability of these catalysts.

## 2. Experimental

### 2.1. Catalyst preparation

Catalyst precursors were prepared by simultaneous precipitation from a mixed aqueous solution of Ni and Al nitrates with sodium carbonate, to produce catalysts with a nominal Ni:Al molar ratio of 3:1. The precipitates were then washed with water, dried at 60 °C (48 h) and at 100 °C (5 h) and calcined in air at 550 °C

* Corresponding author. Tel.: +55 16 33739951; fax: +55 16 33739952.
*E-mail addresses:* sil_maluf@iqsc.usp.br (S.S. Maluf), eassaf@iqsc.usp.br (E.M. Assaf).

0016-2361/$ - see front matter © 2009 Elsevier Ltd. All rights reserved.
doi:10.1016/j.fuel.2009.03.025

(5 h), to obtain the oxide precursor. The Mo was added by impregnation of the oxide precursor with a solution of ammonium heptamolybdate. After drying, the samples (with and without Mo) were again calcined in air at 800 °C (5 h). The content of molybdenum was 0.0%, 0.05%, 0.5%, 1.0% and 2.0% (% w/w).

### 2.2. Characterization of samples

For all the characterization tests described here, samples were in the unreduced oxide form.

The real contents of Ni, Al, Mo and Na were measured in the samples by inductively coupled plasma atomic emission spectroscopy (ICP-AES), with an AtomScan 25 (Thermo Jarrel Ash).

Specific surface area and average pore radius of samples were measured by physical adsorption of $N_2$ (BET method) with a Quantachrome NOVA 2000.

X-ray diffraction (XRD) patterns were collected at room temperature in a URD-6 Carl Zeiss diffractometer with Cu K$\alpha$ radiation (1.54056 Å). The spectra were scanned in the range $2\theta$ = 3–100° at a rate of 3 $min^{-1}$.

Temperature-programmed reduction (TPR) was performed in a quartz tube reactor, using a Micromeritics Chemisorb 2705 instrument. Hydrogen consumption was measured with a thermal conductivity detector (TCD). Fifty milligram of catalyst was placed in the reactor and reduced with a 5% $H_2$–95% He (v/v) gas mixture. The temperature was increased to 1000 °C at a heating rate of 10 °C $min^{-1}$. The amount of $H_2$ consumed was calibrated with a standard CuO powder.

$H_2$ chemisorption experiments were performed after temperature-programmed reduction (TPR). The samples were heated in pure $H_2$ (50 mL $min^{-1}$) at 800 °C for 3 h, then cooled to ambient temperature in a flow of $H_2$ for 1 h, for chemisorption of $H_2$ on the surface of the samples. Excess of $H_2$ was removed in a flow of the He (for 1 h). The sample was then ramped to 650 °C at a linear heating rate of 20 °C $min^{-1}$ in flowing He. $H_2$ was analyzed with a TCD and data were recorded on-line by a computer.

Raman Spectroscopy was carried out with a Jobin-Yvon T64000 spectrometer equipped with an Olympus CCD detector-coupled microscope (micro-Raman). The line at 514.5 nm of an $Ar^+$ laser (73 µW) was used.

X-ray photoelectron spectroscopy (XPS) was performed in ultra-high vacuum, using a Microtech – FISONS Instruments MT 500 VG. An Al K$\alpha$ ($h\nu$ = 1486.6 eV) X-ray source was used, with an emission current of 10 mA at 10 kV. The binding energies were referred to the adventitious hydrocarbon C 1s level set at 284.8 eV.

### 2.3. Catalytic tests

Hundred milligram of catalyst (60–80 mesh) was placed in a vertical fixed-bed quartz reactor (13 mm diameter and 500 mm length) and reduced *in situ* in flowing $H_2$ (50 mL $min^{-1}$) at 800 °C (10 °C $min^{-1}$) for 3 h, to activate the catalyst. The preheated reagents were then fed into the reactor at steam/methane ratios of 4:1 and 2:1 with a $CH_4$ flow of 40 mL $min^{-1}$, $W/F$ = 0.15 g min $mL^{-1}$, and a reaction temperature of 700 °C. All flow was controlled by a set of mass-flow controllers (MKS – 247 four channels). The reactants and the reaction products of the outlet were analyzed in-line by gas chromatography (Varian, Model CP-3800), with two thermal conductivity detectors and an automatic injection valve. One of two streams was used to analyze hydrogen and methane, which were separated in a 13X molecular sieve packed column, with $N_2$ as carrier gas. The other stream was used to analyze $CO_2$, $CH_4$ and CO; He was used as the carrier gas and separation was performed in a 13X molecular sieve and Porapak N packed columns.

Below are the reactions that occur during the steam reforming of methane. The reaction (2.3.3) is the sum of reactions (2.3.1) and (2.3.2):

$$CH_4 + H_2O \rightarrow CO + 3H_2 \quad (2.3.1)$$

$$CO + H_2O \rightarrow CO_2 + H_2 \quad (2.3.2)$$

$$CH_4 + 2H_2O \rightarrow CO_2 + 4H_2 \quad (2.3.3)$$

Assuming the above reactions, the conversions expressed on a dry basis were calculated as follows:

$$X_{CH_4} = \left[\frac{CH_4 \text{ moles reacted}}{CH_4 \text{ moles fed}}\right] = \frac{F^0_{CH_4} - F_{CH_4}}{F^0_{CH_4}} \quad (2.3.4)$$

$$X_{CO_2} = \left[\frac{CO_2 \text{ moles formed}}{CH_4 \text{ moles fed}}\right] \times \frac{1}{3} = \frac{F_{CO_2}}{F^0_{CH_4}} \times \frac{1}{3} \quad (2.3.5)$$

$$X_{CO} = \left[\frac{CO \text{ moles formed}}{CH_4 \text{ moles fed}}\right] \times \frac{1}{3} = \frac{F_{CO}}{F^0_{CH_4}} \times \frac{1}{3} \quad (2.3.6)$$

$$X_{H_2} = \left[\frac{CH_4 \text{ moles reacted}}{CH_4 \text{ moles fed}}\right] \times \frac{2}{3} = \frac{(F^0_{CH_4} - F_{CH_4})}{F^0_{CH_4}} \times \frac{2}{3} \quad (2.3.7)$$

where $F^0_{CH_4}$ = molar flow of $CH_4$ in feed, $F_i$ = molar flow of component $i$ in the output of the chromatograph, $X_{CH_4}$ = $CH_4$ conversion in products, $X_{CO_2}$ = $CO_2$ formation from $CH_4$, $X_{CO}$ = CO formation from $CH_4$, $X_{H_2}$ = $H_2$ formation from $CH_4$.

## 3. Results and discussion

The results of ICP-AES showed that the contents were very close to the nominal composition (Table 1), indicating that there was no loss of Mo by sublimation. This suggests that this method of preparation is suitable.

The total surface area of the catalysts (Table 2) decreased on addition of Mo oxide. This may indicate that the latter was deposited in the narrowest pores, blocking them and effectively raising the average pore diameter. The average pore radius is in the range 45–50 Å, increasing to 60 Å in the samples with 2.0% Mo, indicating the prevalence of mesopores.

In determining the metal surface area (Table 2), a stoichiometric molar ratio of H:Ni = 1:1 and no adsorption of $H_2$ on molybdenum were assumed.

**Table 1**
ICP-AES results for the samples.

| Catalyst | Ni* (%) | Al* (%) | Mo* (%) real | Na (%) |
|---|---|---|---|---|
| Ni/Al | 60.2 ± 1.34 | 8.46 ± 0.74 | – | – |
| 0.05% Mo/Ni/Al | 60.6 ± 1.34 | 8.58 ± 0.08 | 0.049 ± 0.0 | – |
| 0.5% Mo/Ni/Al | 60.9 ± 0.57 | 8.22 ± 0.18 | 0.51 ± 0.01 | – |
| 1.0% Mo/Ni/Al | 59.7 ± 0.14 | 8.43 ± 0.03 | 0.94 ± 0.009 | – |
| 2.0% Mo/Ni/Al | 60.0 ± 0.0 | 8.69 ± 0.0 | 1.96 ± 0.0 | – |

* % w/w.

**Table 2**
Surface and active areas, and average radius of pores.

| Mo (%) | Surface area ($m^2$/g cat) | Active area ($m^2$/g Ni) | Average radius of pores (Å) |
|---|---|---|---|
| 0.0 | 97.9 | 138.2 | 49.1 |
| 0.05 | 97.7 | 36.8 | 49.0 |
| 0.5 | 89.8 | 47.3 | 45.6 |
| 1.0 | 89.3 | 72.7 | 45.9 |
| 2.0 | 78.3 | 73.0 | 64.0 |

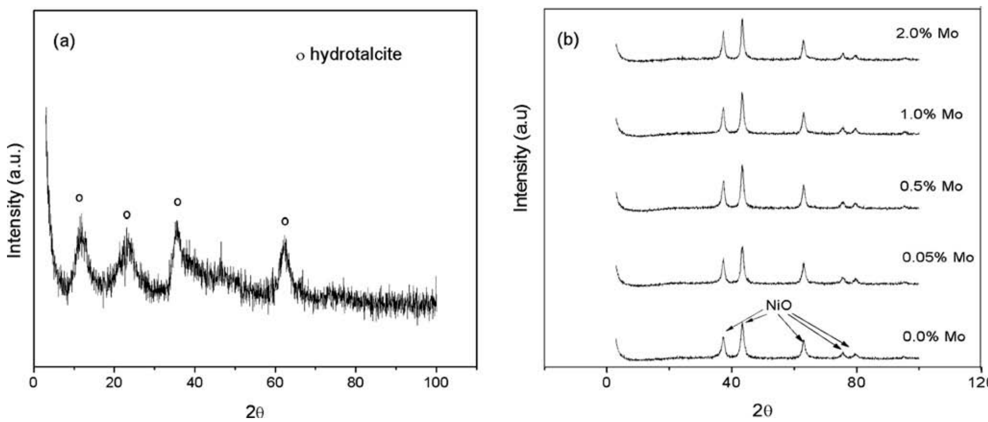


**Fig. 1.** (a) X-ray diffraction pattern of precursors of catalysts; (b) X-ray diffraction patterns of catalysts.

Table 2 shows a decrease of the metal area on addition of 0.05% molybdenum. This effect became less pronounced as more Mo was added, corroborating the behavior of catalyst prepared by Borowiecki [12–14].

This decline in metal area may be caused in many ways: sintering during the thermal treatments of catalysts or formation of Ni–Mo–O compounds which may have a higher thermal stability, converting elemental Ni to combined species; segregation of the NiO phase in the presence of molybdenum, forming large particles and generating a lower area. Aksoyluand and Őnsan [15] reported that the addition of Mo promoted a reduced metal area because the Ni species were covered by $MoO_x$ species, in Ni–Mo/$\gamma$-$Al_2O_3$ catalysts.

### 3.1. X-ray diffraction

Fig. 1a displays the X-ray pattern of the precursor and this result shows the presence of a hydrotalcite (JCPDS #41-1428) structure with broad peaks indicating low crystallinity. There are two signals (at 40° and 45°) of low intensity that are assigned to nickel hydroxide (JCPDS #74-2075). This compound was expected because it has been shown that for Ni:Al molar ratios between 2 and 3, the precursor exhibits the structure hydrotalcite together with Ni and/or Al hydroxides [16].

The X-ray diffraction patterns of the catalysts, which show a more crystalline structure than the precursors, are displayed in Fig. 1b. The signals showed the presence of NiO (JCPDS # 78-0643) in the structure of the samples. However, the main peaks of aluminate (JCPDS # 77-1877) coincide with the main peaks of NiO observed in Fig. 1b. Thus, the 37° and 45° peaks in Fig. 1b may be the sum of the peaks of NiO and aluminate.

The catalysts prepared here generated stronger and better defined peaks than those seen in patterns for samples prepared by the same method, but with a molar ratio Ni:Al = 1.5:1, published in a previous study [17]. This shows that increasing the nickel load resulted in a rise in crystallinity, whereas the presence of molybdenum caused no detectable change in the X-ray diffraction patterns.

No reflection originating from molybdenum oxides or nickel molybdate was detected, because of the low content of Mo.

### 3.2. Temperature-programmed reduction (TPR)

TPR profiles of the catalysts are plotted in Fig. 2. For the catalyst without Mo promoter, there is a reduction peak starting at 450 °C, with a maximum at 800 °C and a shoulder at 580 °C.

The reduction of NiO interacting weakly with the support occurs at 450 °C [18]. The signal at 800 °C refers to reduction of a $NiO$–$Al_2O_3$ phase similar to bulk $NiAl_2O_4$ [18–20], although this structure was not identified in the XRD results, presumably because it is highly dispersed in the structure of the catalysts.

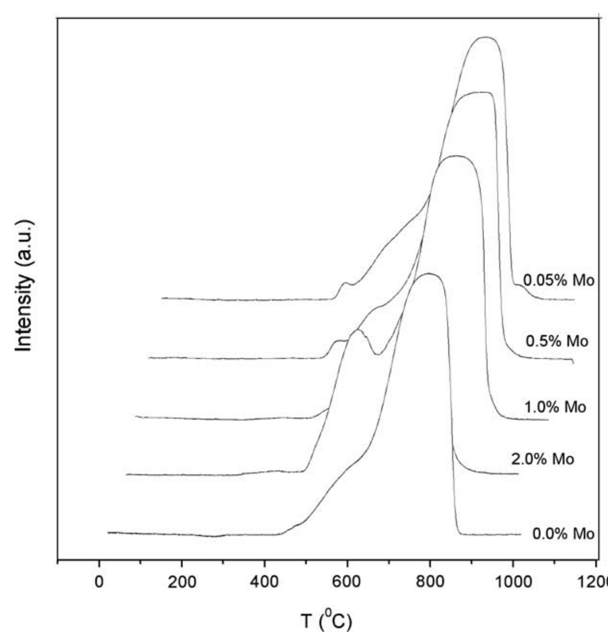


**Fig. 2.** TPR profiles of catalysts.

Young et al. [19] suggested that the signal at 580 °C refers to the reduction of nickel species forming a surface phase with the support, in which $Ni^{2+}$ cations are in octahedral coordination, while Teixeira and Giudici [18] suggests the formation of compounds similar to non-stoichiometric nickel aluminate.

The catalysts promoted with molybdenum, up to 2.0%, have TPR profiles quite similar to the catalyst without molybdenum. However, the catalysts with 0.05% and 0.5% Mo have a small peak at 460 °C, which refers to the reduction of less stable NiO, i.e., $Ni^{2+}$ species that interact weakly with the support.

For catalysts with 1.0% Mo, the peak at 460 °C disappears and for catalysts with 2.0% Mo, this peak fuses with the shoulder at 580 °C, forming a peak at 600 °C, which suggests that less thermally stable $NiO$–$Al_2O_3$ compounds are formed. Also, the sample with 2.0% Mo has the maximum of the peak shifted to lower temperature, as reported by Laniecki et al. [21].

In relation to species formed with molybdenum, the stronger peak for the catalyst with 2.0% Mo could also be a consequence

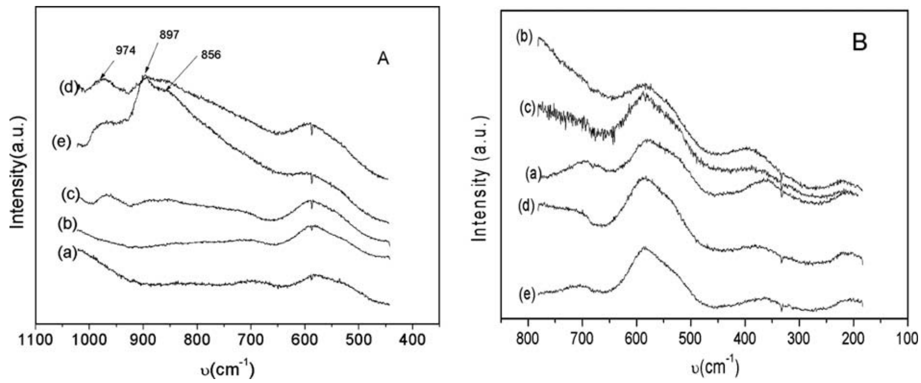


**Fig. 3.** (a) Raman spectra of catalysts in the range 800–200 $cm^{-1}$; (b) Raman spectra of catalysts in the range 1100–400 $cm^{-1}$.

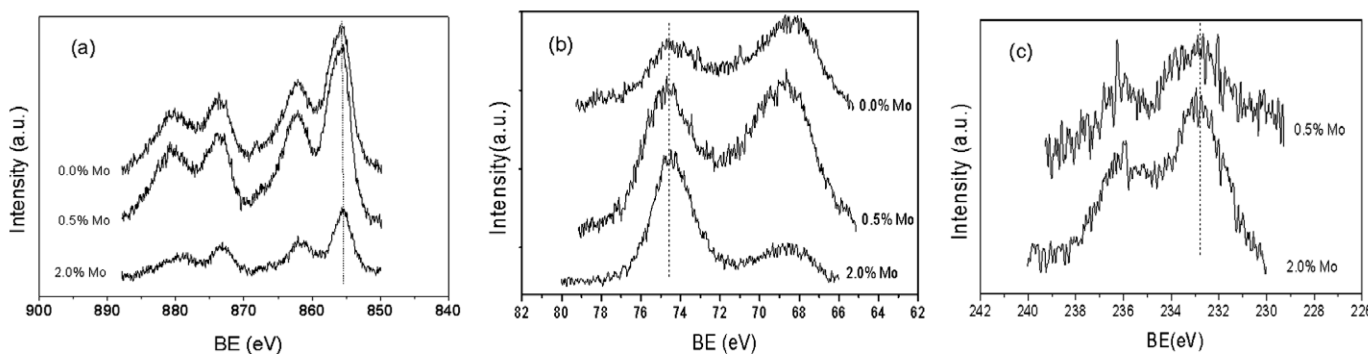


**Fig. 4.** (a) XPS spectra for a Ni 2p, (b) Al 2p, (c) Mo 3d of catalysts.

of reduction of $Mo^{6+}$ to $Mo^{4+}$ in a Ni–Mo–O phase, or simultaneous reduction with nickel [21].

### 3.3. Raman Spectroscopy

The Raman spectra of the $Mo/Ni/Al_2O_3$ catalysts are shown in Fig. 3a and b.

In Fig. 3a, all spectra have two broad and low intensity bands: one at 500–650 $cm^{-1}$ and the other at 300–400 $cm^{-1}$. Both bands are associated with vibrations of $NiAl_2O_4$ [22,23]. No signal characteristic of NiO (500 $cm^{-1}$) was observed, suggesting that there is no NiO at the surface. Probably, NiO species diffuse into the support of bulk $NiAl_2O_4$ during the high-temperature treatment. This result is consistent with those in the literature [22,23].

The spectra, in the range from 1100 to 400 $cm^{-1}$ (Fig. 3b), have two shoulders at 856 and 974 $cm^{-1}$ and a signal at 897 $cm^{-1}$, for samples with Mo contents higher than 0.05%. According to the literature [24,25], the signals at 897 and 974 $cm^{-1}$ are due to the presence of tetrahedral $MoO_4^{-2}$. Salerno et al. [26] suggest that weak bands near 960 and 870 $cm^{-1}$ are due to the presence of $MoO_x$ species and some alkali molybdates. Dufresne et al. [22] observed a broad line at 940–950 $cm^{-1}$ with a shoulder at 780–840 $cm^{-1}$, assigned to tetrahedral molybdate species, distorted by multiple interactions, in $MoO_3/\gamma$-$Al_2O_3$ and $Ni/MoO_3/\gamma$-$Al_2O_3$ catalysts.

The presence of $MoO_4^{-2}$ species in the structure of the catalysts studied here is due to the use of small amounts of Mo, which favors the presence of molybdates [27]. However, no comment can be made on the type of molybdate, because they could not be identified, mainly because of the low Mo contents.

### 3.4. X-ray photoelectron spectroscopy (XPS)

Fig. 4 displays XPS spectra for Ni 2p, Al 2p and Mo 3d and Table 3 shows the binding energy (BE) of metals analyzed for each sample.

The BEs of Ni $2p_{3/2}$ in the catalysts (Table 3) were similar to those of Ni in the form $NiAl_2O_4$ or $Ni_2O_3$, according to the literature [28]. The signal for NiO (854.0 eV) was not seen.

Dufresne et al. [22], in a study of Ni–Mo/$\gamma$-$Al_2O_3$ catalysts, also noted a lack of NiO species and Ni2$p_{3/2}$ spectra were similar to those for $NiAl_2O_4$.

In Ni/$\gamma$-$Al_2O_3$ samples with more than 8.0% Ni, Mérida et al. [29] reported two signals for $Ni^{2+}$ species: one at 854.1 eV for octahedrally coordinated $Ni^{2+}$ present in the supported NiO structure, the other at 856.1 eV, associated with $Ni^{2+}$ in octahedral sites in the spinel structure which results from the solid state reaction between oxides of nickel and aluminum during calcination.

In order to confirm the presence of $NiAl_2O_4$, the Al 2p spectra were recorded (Fig. 4b) and the BE values (Table 3) confirmed the presence of $NiAl_2O_4$ [28] at the surface.

**Table 3**
Values of BE of catalysts.

| %Mo | Binding energy (eV) | | |
|---|---|---|---|
| | Ni $2p_{3/2}$ | Al 2p | Mo 3d |
| 0.0 | 855.8 | 73.6 | – |
| 0.5 | 855.6 | 74.6 | 232.8 |
| 2.0 | 855.5 | 74.5 | 232.9 |

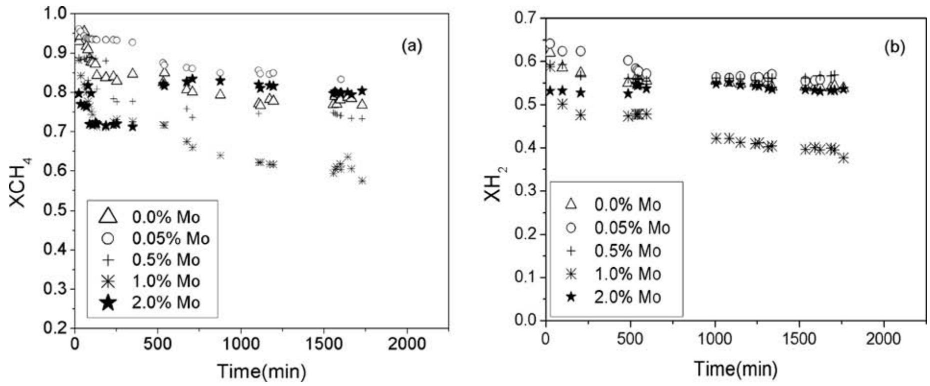


**Fig. 5.** (a) Total conversion of $CH_4$ (steam/methane = 4:1); (b) yield to $H_2$ (steam/methane = 4:1).

According to the literature [28], the BE values of Mo $3d_{5/2}$ (Table 3) showed the presence of $Mo^{6+}$ ions on the catalyst surface [24,30,31]. In relation to this form of molybdenum, Barath et al. [32] suggests the presence of $MoO_3$.

Dufresne et al. [22] obtained a signal at 856.7 eV for the Ni 2p spectra of $NiMoO_4$. This signal coincides with that for Ni in the Ni 2p spectra in our results, which may indicate the presence of $MoO_4^{-2}$ species here, because our Raman spectra also suggest the presence of these species.

### *3.5. Catalytic tests*

#### *3.5.1. Feed of steam/methane = 4:1*

The catalytic activity for the higher ratio of steam to methane is plotted in Fig. 5a.

In the tests of the catalyst without molybdenum, deactivation was not observed and the methane conversion was stable around 85% for nearly 30 h (Fig. 5a). The addition of molybdenum did not modify this behavior and the promoted catalysts also suffered no deactivation up to 30 h on line, with one exception. Only in the catalyst with 1.0% Mo did the initial activity decrease by ~20%, ending up with a conversion of 65%.

The rate of conversion of $CH_4$ to $H_2$ (Fig. 5b) remained unchanged at around 55% with the addition of molybdenum, with the exception of the samples with 1.0% Mo, which showed lower conversion rates (45%).

The conversion to CO remained constant (Fig. 6a) around 5%. Conversion to $CO_2$ (Fig. 6b) increased from 15% to 20%, for the catalyst with 0.05% Mo, and then fell to 10% as the load of Mo increased to 2.0%. Thus, the addition of a small amount of Mo seems to have a positive effect on the water–gas shift reaction (reaction (2)), favoring the formation of $CO_2$.

#### *3.5.2. Feed of steam/methane = 2:1*

The results for reactions with a feed of 2:1 steam/methane are shown in Figs. 7 and 8.

The catalysts with 0.0% Mo were active for a few hours (200 min), as shown in Fig. 7a, contrary to previous results with the lower molar ratio of steam [17], in which catalysts with a lower molar ratio of Ni and 0.0% Mo showed no activity for a feed of steam/methane = 2:1. The present activity may be due to the higher content of Ni and thus a greater number of active sites available, delaying the deactivation of the catalysts.

Fig. 7a shows a decrease in the $CH_4$ conversion to around 65% for the catalysts containing Mo, contrasting with the results obtained with the same catalysts in the experiments with a 4:1 feed ratio (Fig. 5a).

The catalyst containing 0.05% Mo (Fig. 7a) exhibited a stable conversion of 60% for 500 min, with an initial conversion of $CH_4$ around 80%. This shows that low levels of Mo combined with a small amount of Ni improve the stability of the catalyst, which forms less carbon than catalyst without molybdenum [12].

With the other catalysts, it was possible to continue the catalytic test for ~350–400 min, during which the conversion remained at the same level as that of the catalyst with 0.05% Mo. After this time, carbon deposits were formed, which blocked the catalytic bed, generating high pressures inside the reactor.

Fig. 7b shows the conversion of $CH_4$ to $H_2$ and this remained at 45%, lower than the value obtained at the higher steam/methane ratio, and the total conversion of $CH_4$ is also lower with the feed ration steam/methane = 2:1.

With respect to conversions to $CO_2$ and CO (Fig. 8a and b), the catalysts showed the same behavior as when they were tested with a feed of steam/methane = 4:1.

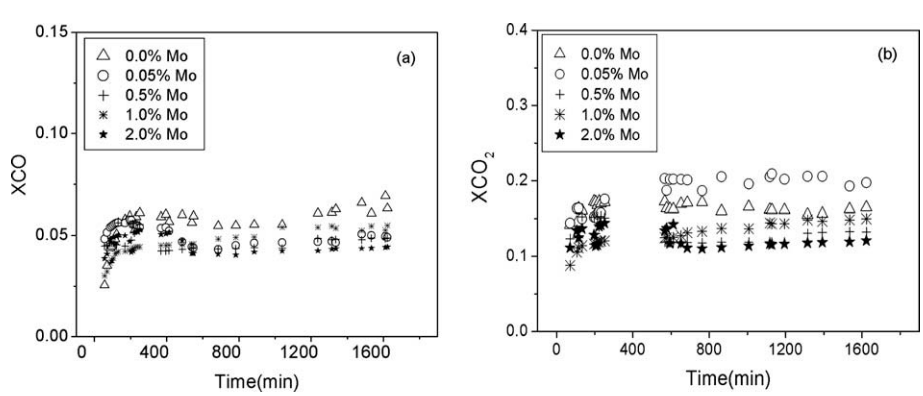


**Fig. 6.** (a) Conversion of $CH_4$ to CO (steam/methane = 4:1); (b) yield to $CO_2$ (steam/methane = 4:1).

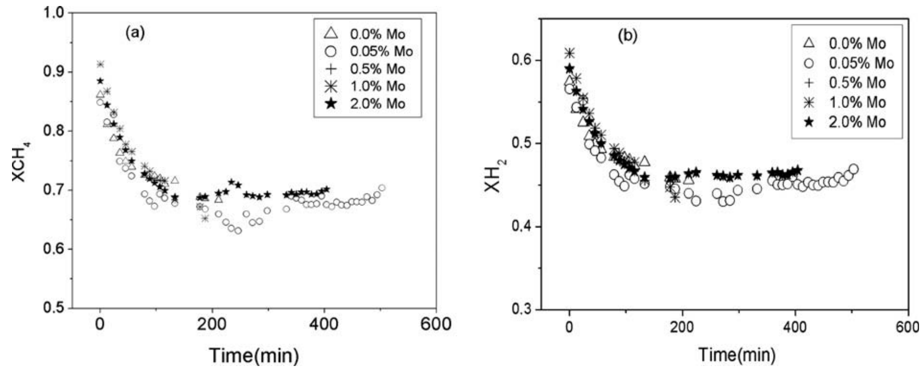


**Fig. 7.** (a) Total conversion of $CH_4$ (steam/methane = 2:1); (b) yield to $H_2$ (steam/methane = 2:1).

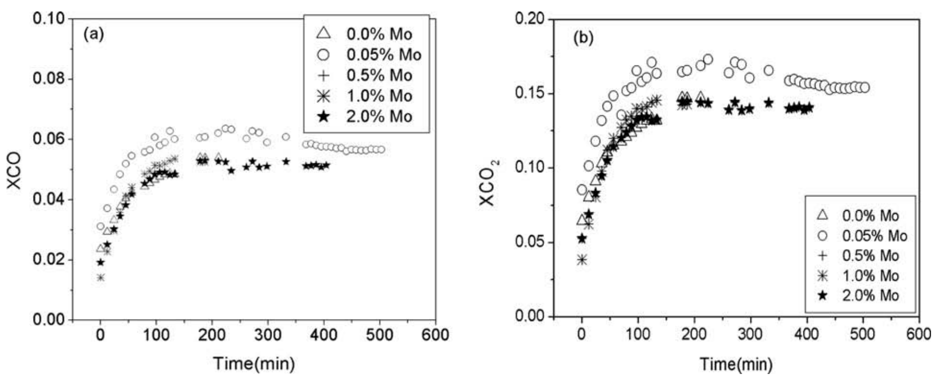


**Fig. 8.** (a) Yield to $CO_2$ (steam/methane = 2:1); (b) yield to CO (steam/methane = 2/1).

As a general comparison of the results obtained at the two feed molar ratios, it can be said that the conversion of $CH_4$ is lower and the catalyst remains active only until 400 min at the steam/methane molar ratio of 2:1. The same is true of conversion to $H_2$, CO and $CO_2$.

### *3.6. Effect of level of Mo on metal area and specific activity*

In Fig. 9a and b, the metallic area and specific activity, respectively, of the catalytic sites for the reform reaction are plotted against the molybdenum load.

It can be seen that the area of metal on all the catalysts with molybdenum is lower than on the catalyst without Mo (Fig. 9a). This is indicative that the promoter does not have a textural effect, because this effect would cause a decreasing of the size in Ni sites and consequently an increase in total metallic area, by dissolution of $Mo^{6+}$ species in the $Ni/Al_2O_3$ matrix.

The decline in metallic area may be caused in many ways: sintering during the thermal treatment of catalysts (as previously mentioned with regard to TPR results); formation of Ni–Mo–O compounds which may have higher thermal stability, converting elemental Ni to combined species; segregation of the NiO phase in the presence of molybdenum, forming large particles no stabilized and generating a lower area.

The catalyst with 0.05% Mo showed the lowest metallic area, probably because of the NiO segregation effect, since TPR results showed the presence of peak at 460 °C, assigned to less stable $Ni^{+2}$ species. Ni–Mo–O compounds are not formed because these compounds are not found in the Raman results for the sample with 0.05% Mo. This explanation could not be confirmed by XPS since it was not possible to perform this analysis on this sample, because its Mo content was very low.

Fig. 9b shows the activity is highest when the metallic area is smallest, namely in the sample with 0.05% Mo. This indicates that

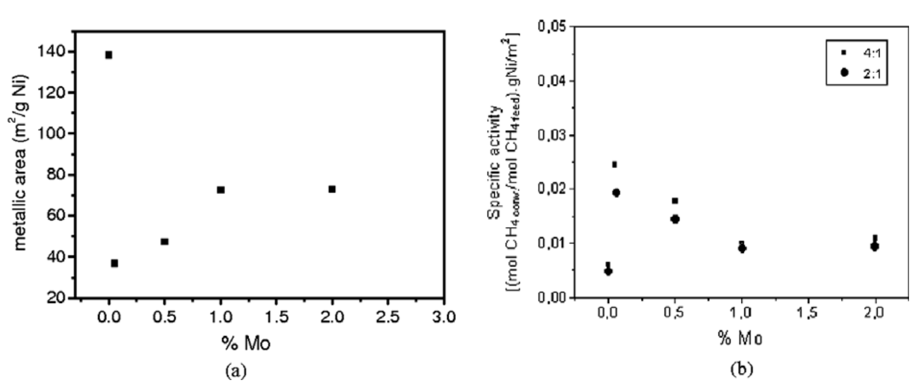


**Fig. 9.** (a) Metal area vs. Mo content of catalysts; (b) specific activity vs. Mo content.

a smaller number of sites are available for reaction in this sample but that these sites are more active. In Fig. 9b, the catalysts with 0.05% had the higher specific activity. According to Aksoylu and Őnsan [17,18], an increase of specific activity, despite a fall in the metallic area,, is an sign of the transfer of electrons from $MoO_x$ species to Ni particles, causing a rise in turnover frequency, TOF (the maximum number of molecules of substrate that a catalyst can convert to product per catalytic site per unit time).

## 4. Conclusion

- X-ray diffraction and TPR analysis showed that the samples have two phases in the bulk: NiO and $NiAl_2O_4$.
- XPS and Raman spectroscopy showed the presence of $Ni_2AlO_4$ and/or $Ni_2O_3$ and $MoO_4^{-2}$ on the surface.
- With a feed of steam/methane = 2:1, it was possible to test the catalysts for approximately 400 min, until they were blocked, and the rates of $CH_4$ conversion to $CO_2$, CO and $H_2$ were lower than the values obtained with a feed of steam/methane = 4:1.
- The addition of Mo decreased the surface metal area, but increased the specific activity of the active sites. This is an indication of the transfer of electrons from $MoO_x$ species to Ni, leading to an increase in the electron density of metallic Ni.
- The decrease in the number of sites may also be due to blockage of the active Ni species by $MoO_x$.

## Acknowledgements

The authors thank FAPESP for financial assistance, IF/UNICAMP for Raman and XPS analyses and DEQ/UFSCar for the BET and XRD analyses.

## References

[1] Simpson AP, Lutz AE. Energy analysis of hydrogen production via steam methane reforming. Int J Hydrogen Energy 2007;32:4811–20.
[2] Yu W et al. A comparative simulation study of methane steam reforming in a porous ceramic membrane reactor using nitrogen and steam as sweep gases. Int J Hydrogen Energy 2008;33:685–92.
[3] Midilli A, Ay M, Dincer I, Rosen MA. On hydrogen and hydrogen energy strategies. I: Current status and needs. Renew Sustain Energy Rev 2005;9:255–71.
[4] Caillot T, Gélin P, Dailly J, Gauthier G, Cayron C, Laurencin J. Catalytic steam reforming of methane over $La_{0.8}Sr_{0.2}CrO_3$ based Ru catalysts. Catal Today 2007;28:264–8.
[5] Bonura G, Di Blasi O, Spadaro L, Arena F, Frusteri F. A basic assessment of the reactivity of Ni catalysts in the decomposition of methane for the production of "$CO_x$-free" hydrogen for fuel cells application. Catal Today 2006;116:298–303.
[6] Monzon A et al. Improvement of activity and stability of Ni–Mg–Al catalysts by Cu addition during hydrogen production by catalytic decomposition of methane. Catal Today 2006;16:264–70.
[7] Suelves I, Lazaro MJ, Moliner R, Echegoyen Y, Palacios JM. Characterization of NiAl and NiCuAl catalysts prepared by different methods for hydrogen production by thermo-catalytic decomposition of methane. Catal Today 2006;116:271–80.
[8] Kugai J, Subramani V, Song C, Engelhard MH, Chin YH. Effects of nanocrystalline $CeO_2$ supports on the properties and performance of Ni–Rh bimetallic catalyst for oxidative steam reforming of ethanol. J Catal 2006;238:430–40.
[9] Fierro V, Akdim O, Provendier H, Mirodatos C. Ethanol oxidative steam reforming over Ni-based catalysts. J Power Sources 2005;145:659–66.
[10] Borowiecki T, Gac W, Gotebiowski A. Effects of small $MoO_3$ additions on the properties of nickel catalysts for the steam reforming of hydrocarbons. III: Reduction of Ni–$Mo/Al_2O_3$ catalysts. Appl Catal A 2004;270:27–36.
[11] Borowiecki T, Giecko G, Panczyk M. Effects of small $MoO_3$ additions on the properties of nickel catalysts for the steam reforming of hydrocarbons. II: Ni–$Mo/Al_2O_3$ catalysts in reforming, hydrogenolysis and cracking of *n*-butane. Appl Catal A 2002;230:85–97.
[12] Borowiecki T, Golebiowski A, Ryczkowski J, Stasinska B. The influence of promoters on the coking rate of nickel catalysts in the steam reforming of hydrocarbons. Stud Surf Sci Catal 1999;119:711–6.
[13] Borowiecki T, Golebiowski A. Influence of molybdenum and tungsten additives on the properties of nickel steam reforming catalysts. Catal Lett 1994;25:309–13.
[14] Kepinski L, Stasinska T, Borowiecki T. Carbon deposition on $Ni/Al_2O_3$ catalysts doped with small amounts of molybdenum. Carbon 2000;38:1845–56.
[15] Aksoylu AE, Őnsan IZ. Interaction between nickel and molybdenum in Ni–Mo/ catalysts. II: CO hydrogenation. Appl Catal A 1998;168:399–407.
[16] Puxley DC, Kitchener IJ, Komodromos C, Parkins ND. The effect of preparation method upon the structures, stability and metal interactions in nickel/alumina catalysts. Amsterdam: Elsevier Science Publishers; 1983.
[17] Maluf SS, Assaf EM, Assaf JM. Catalisadores $Ni/Al_2O_3$ Promovidos com Molibdênio para a Reação de Reforma a Vapor de Metano. Quim Nova 2003;26:181–7.
[18] Teixeira ACSC, Giudici R. Deactivation of steam reforming catalysts by sintering: experiments and simulation. Chem Eng Sci 1999;54:3609–18.
[19] Young CP, Eun S, Hyun KR. Characterization and catalytic activity of WNiMo/ $Al_2O_3$ catalysts for hydrodenitrogenation of pyridine. Ind Eng Chem Res 1997;36:5083–9.
[20] Cordero RL, Agudo AL. Effect of water extraction on the surface properties of $Mo/Al_2O_3$ and $Ni/Mo/Al_2O_3$ hydrotreating catalysts. Appl Catal A 2000;202:23–35.
[21] Laniecki M, Malecka-Grycz M, Domka F. Water–gas shift reaction over sulfided molybdenum catalysts. I: Alumina, titânia and zirconia-supported catalysts. Appl Catal A 2000;196:293–303.
[22] Dufresne P, Payen E, Grimblot J, Bonnelle JP. Study of Ni–Mo–y-$Al_2O_3$ catalysts by X-ray photoelectron and Raman spectroscopy. Comparison with Co–Mo–y–$Al_2O_3$ catalysts. J Phys Chem 1981;85:2344–51.
[23] Aminzadeh A, Sarikhani-Fard H. Raman spectroscopic study of $Ni/Al_2O_3$ catalyst. Spectrochim Acta A 1999;55:421–1425.
[24] Andonova S, Vladov Ch, Pawelec B, Shtereva I, Tyuliev G, Damyanova S, et al. Effect of the modified support $\gamma$-$Al_2O_3$–CaO on the structure and hydrodesulfurization activity of Mo and Ni–Mo catalysts. Appl Catal A 2007;328:201–9.
[25] Sardhar Basha SJ, Sasirekha NR, Maheswari R, Shanthi K. Mesoporous. H-AlMCM-41 supported NiO–$MoO_3$ catalysts for hydrodenitrogenation of *o*-toluidine. I: Effect of $MoO_3$ Loading. Appl Catal A 2006;308:91–8.
[26] Salerno P, Mendioroz S, López Agudo A. Al-pillared montmorillonite-based NiMo catalysts for HDS and HDN of gas oil: influence of the method and order of Mo and Ni impregnation. Appl Catal A 2004;259:17–28.
[27] Mestl G, Srinivasan TK. Raman spectroscopy of monolayer-type catalysts: supported molybdenum oxides. Catal Rev Sci Eng 1998;40:451–570.
[28] Moulder J, Stickle WF, Sobol PE, Bomben KD. Handbook of X-ray photoelectron on spectroscopy. 2nd ed. USA: Perkin–Elmer Corporation; 1992.
[29] Mérida RJ, Rodríguez CE, Jiménez LA. Characterization of Ni, Mo and Ni–Mo catalysts supported on alumina-pillared $\alpha$-zirconium phosphate and reactivity for the thiophene HDS reaction. J Mol Catal A Chem 1999;145:169–81.
[30] Venezia AM. X-ray photoelectron spectroscopy (XPS) for catalysts characterization. Catal Today 2003;77:359–70.
[31] Li J, Xiang L, Feng X, Wang Z. Influence of hydrothermally modified $\gamma$-$Al_2O_3$ on the properties of NiMo/$\gamma$-$Al_2O_3$ catalyst. Appl Surf Sci 2008;254:2077–80.
[32] Barath F, Turki M, Keller V, Maire G. Catalytic activity of reduced $MoO_3/\alpha$-$Al_2O_3$ for hexanes reforming. J Catal 1999;185:1–11.